The Impact of Climate Change on Air Quality–Related Meteorological Conditions in California. Part I: Present Time Simulation Analysis

ZHAN ZHAO

Department of Land, Air, and Water Resources, University of California, Davis, Davis, and Scripps Institution of Oceanography, University of California, San Diego, La Jolla, California

SHU-HUA CHEN

Department of Land, Air, and Water Resources, University of California, Davis, Davis, California

MICHAEL J. KLEEMAN

Department of Civil and Environmental Engineering, University of California, Davis, Davis, California

MARY TYREE AND DAN CAYAN

Scripps Institution of Oceanography, University of California, San Diego, La Jolla, California

(Manuscript received 14 May 2010, in final form 2 December 2010)

ABSTRACT

This study investigates the impacts of climate change on meteorology and air quality conditions in California by dynamically downscaling Parallel Climate Model (PCM) data to high resolution (4 km) using the Weather Research and Forecast (WRF) model. This paper evaluates the present years' (2000–06) downscaling results driven by either PCM or National Centers for Environmental Prediction (NCEP) Global Forecasting System (GFS) reanalysis data. The analyses focused on the air quality–related meteorological variables, such as planetary boundary layer height (PBLH), surface temperature, and wind. The differences of the climatology from the two sets of downscaling simulations and the driving global datasets were compared, which illustrated that most of the biases of the downscaling results were inherited from the driving global climate model (GCM). The downscaling process added mesoscale features but also introduced extra biases into the driving global data. The main source of bias in the PCM data is an imprecise prediction of the location and strength of the Pacific subtropical high (PSH). The analysis implied that using simulation results driven by PCM data as the input for air quality models will likely underestimate air pollution problems in California. Regional-averaged statistics of the downscaling results were estimated for two highly polluted areas, the South Coast Air Basin (SoCAB) and the San Joaquin Valley (SJV), by comparing to observations. The simulations driven by GFS data overestimated surface temperature and wind speed for most of the year, indicating that WRF has systematic errors in these two regions. The simulation matched the observations better during summer than winter in terms of bias. WRF has difficulty reproducing weak surface wind, which normally happens during stagnation events in these two regions. The shallow summer PBLH in the Central Valley is caused by the dominance of high pressure systems over the valley and the strong valley wind during summer. The change of meteorology and air quality in California due to climate change will be explored in Part II of this study, which compares the future (2047–53) and present (2000–06) simulation results driven by PCM data and is presented in a separate paper.

1. Introduction

Because of its geographical location, complex topography, diverse ecosystems, intricate mesoscale meteorological features, and a large amount of pollutant

Corresponding author address: Dr. Shu-Hua Chen, Department of Land, Air, and Water Resources, University of California, Davis, One Shields Ave., Davis, CA 95616.
E-mail: shachen@ucdavis.edu

DOI: 10.1175/2011JCLI3849.1

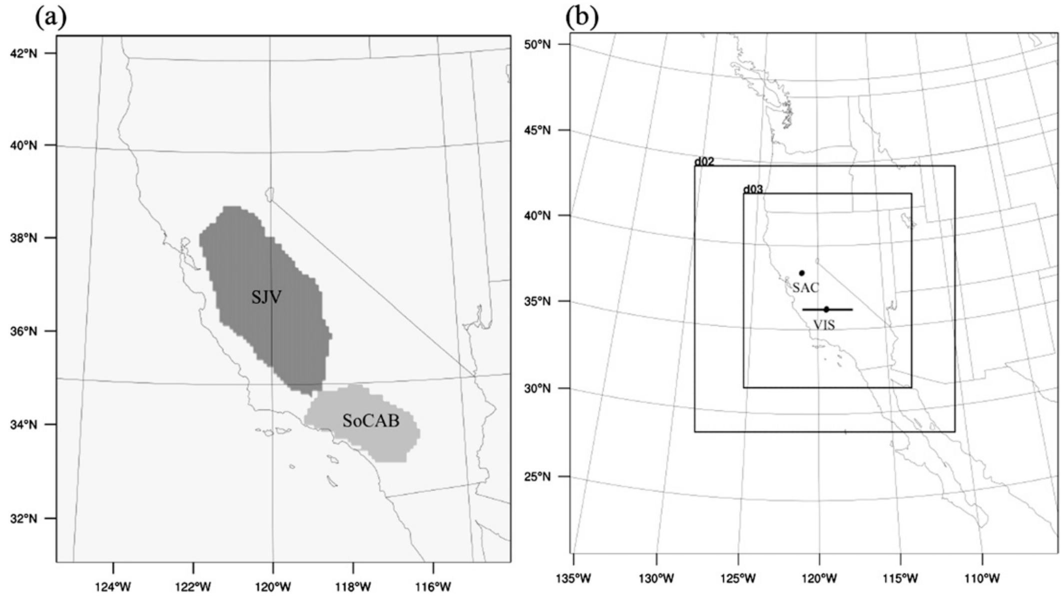

FIG. 1. (a) Locations of SJV and SoCAB in CA. (b) Nested domains for WRF simulations. The black dots show the locations of the observation stations "VIS" and "SAC." The line in domain 3 (d3) crossing VIS indicates the location of the vertical cross section in Fig. 14.

emissions, California (CA) is more vulnerable to climate change than other areas in the United States (Snyder et al. 2002; Leung and Gustafson 2005). For more than a decade, CA has had serious summer ozone and winter particulate matter (PM) problems, especially in the San Joaquin Valley (SJV) and the South Coast Air Basin (SoCAB) (Fig. 1a). The annual average $PM_{2.5}$ concentration in SJV and SoCAB were 21.5 μg m^{-3} and 19.7 μg m^{-3}, respectively, during 2007/08. These concentrations were the highest nationwide (Mahmud et al. 2010) and were much higher than the current National Ambient Air Quality Standard of 15 μg m^{-3}. In the years 2005–07, all of the "top six" counties with the highest O_3 concentrations over the entire United States were located in SJV and SoCAB (Howard et al. 2010). The pollutants in SJV are mainly products of fuel combustion by automobiles and agricultural operations; the prevailing wind also brings pollutant emissions from the San Francisco Bay Area into the valley through the Carquinez Strait. These pollutants are difficult to ventilate out of the valley because of the surrounding mountains. Stagnation events, which are characterized by a shallow mixing layer and low surface wind, occur in SJV during winter and summer. In addition, the development of the boundary layer in SJV is suppressed by the subsiding air associated with the valley wind during summer. Thus, the pollutants are trapped close to the surface. In SoCAB, there are large amounts of pollutant emissions from fuel combustion processes and other human activities in Los Angeles. The presence of a marine atmospheric boundary layer (MABL) inversion in the coastal region of CA, formed by the heated subsiding air associated with Pacific subtropical high (PSH) and the low sea surface temperature (SST) attributed to the coastal ocean upwelling, is also a key factor for the air pollution problem in this region.

It is important to explore the future meteorology and air quality conditions in CA to assess their societal impacts and evaluate control strategies. By downscaling global climate model (GCM) simulations to high-resolution outputs, previous studies have shown that climate change could induce changes in temperature, humidity, precipitation, boundary layer mixing depth, etc., at regional scales and, consequently, cause changes in regional air quality. Previous work in CA has used statistical downscaling to study climate change impacts on air quality (Mahmud et al. 2008; Tagaris et al. 2007). Statistical downscaling methods (Wilby et al. 1998; Zorita and von Storch 1999) downscale GCM variables directly to finer resolution with much higher efficiency than dynamical downscaling. However, because the statistical relationships vary over different air basins, downscaled results are less reliable than those from dynamical downscaling unless sufficient observations are available. To date, the finest resolutions to which GCM variables have been downscaled for regional air quality responses to climate change have been by Jacobson (2008, 2010), who examined feedbacks from climate and air pollution to agriculture and local CO_2 forcing with a resolution of $0.20° \times 0.15°$ in CA and $0.045° \times 0.05°$ in Los Angeles.

However, these two studies spanned a relatively short time period (i.e., one month in Jacobson 2008, and six months for Los Angeles domain and two years for the CA domain in Jacobson 2010). Caldwell et al. (2009) used the Weather Research and Forecasting (WRF) model to dynamically downscale Community Climate System Model version 3 (CCSM3) data to 12-km horizontal resolution for a 40-yr current period in CA with fixed greenhouse gas concentrations. Their analyses focused on precipitation, surface temperature, and snowpack, showing that the WRF model has an internal problem that prevents accurate predictions of precipitation in this region. However, the surface temperature predictions matched observations well. Both Bell et al. (2004) and Leung and Ghan (1999) studied changes in temperature and precipitation extremes in CA under a scenario of doubled CO_2 concentration. Duffy et al. (2006) compared downscaling results from four combinations of regional climate models (RCMs) and GCMs for the western United States and found that the spatial distribution of the meteorological variables can vary substantially among different RCMs owing to different physics processes and surface forcing. All of these studies have shown that biases in downscaled results are largely inherited from the driving GCM. California has particularly complex topography, which interacts with large-, meso, and microscale flow patterns. It is difficult to capture such comprehensive mesoscale features with a RCM at relatively coarse resolutions. To improve the RCM downscaling results in this region, simulations with finer spatial resolution are required.

In this study, the WRF model was applied to dynamically downscale Parallel Climate Model (PCM) (Washington et al. 2000) outputs under a business as usual (BAU) scenario to 4-km resolution in CA. To the best of our knowledge, there are no other dynamical downscaling studies using the WRF model with such a fine resolution to explore the climate change impacts in this region. Two 7-yr periods (2000–06 and 2047–53) have been chosen to study the influence of climate change projections on meteorological variables relevant to air quality. PCM has been reported to have low sensitivity to increased atmospheric CO_2 (Barnett et al. 2001; Duffy et al. 2006). However, it was argued that models with higher climate sensitivity might have difficulty satisfying the ocean constraint (Barnett et al. 2001). Thus, a time interval of approximately 50 years was set between the current and future simulations in this study to have a long enough study period for climate changes to manifest. The ultimate goal of this study is to investigate future air quality in CA, thus the analyses are focused on air quality–related variables, such as 10-m wind speed (wsp10), 2-m temperature (T2), planetary boundary layer height (PBLH), total days, and strength of stagnation events, etc. As mentioned previously, error in the RCM downscaling results partially succeed from GCM bias. To assess the effect of PCM data bias on the WRF downscaling results, a counterpart of the present downscaling simulations (2000–06) was conducted with the same model configuration but driven by Global Forecasting System (GFS) reanalysis data. As Part I of this study, this paper analyzes the current 7-yr climate (2000–06) with intercomparisons between GFS and PCM data as well as their downscaling results for the highly polluted SoCAB and SJV. During the analysis, it was noticed that the summertime PBLH is exceptionally shallow in SJV. This phenomenon was studied and the possible reasons were explored. Part II of this study, which is presented in a separate paper (Zhao et al. 2011), compares present and future simulations driven by PCM data to evaluate the impacts of climate change on meteorological conditions related to air quality, including land–sea breeze, in CA.

The paper is organized as follows. The methodology and numerical models are described in section 2. Section 3 presents the selection of an optimal suite of physics schemes for the region of interest. Section 4 contains the comparison of the simulation results for the present time period driven by PCM and GFS data, as well as an investigation of the summertime low PBLH phenomenon in SJV. Conclusions and remarks follow at the end.

2. Methodology and model description

a. Methodology

Dynamical downscaling uses an RCM to obtain regional-scale, fine-resolution climate change information from a coarse-resolution GCM (i.e., GCM data provide the initial and lateral boundary conditions for the RCM). This method maintains the large-scale features of the climate projection from the GCM and adds a more detailed depiction of mesoscale features (Hay and Clark 2003). Dynamical downscaling can thus be used to investigate the impacts of climate change on meteorology and air quality in specific areas. In this study, WRF model (Skamarock et al. 2007), a community mesoscale meteorology model, was applied to dynamically downscale PCM data under the BAU future forcing scenario (Dai et al. 2001) to investigate the meteorological conditions and their changes in CA, especially SJV and SoCAB. As described in the introduction, the air quality in SJV and SoCAB are largely influenced by mesoscale systems (i.e., valley wind, stagnation events, MABL, etc.), which are not resolved by the coarse spatial ($2.8° \times 2.8°$) and temporal (6 hourly) resolutions of PCM. The WRF simulations with much finer resolution add substantive

TABLE 1. Dates (mm/dd) for simulation cases for normal and leap years.

	Case 1	Case 2	Case 3	Case 4	Case 5	Case 6	Case 7	Case 8	Case 9
Normal years	1/1–1/18	2/12–3/1	3/26–4/12	5/7–5/24	6/18–7/5	7/30–8/16	9/10–9/27	10/22–11/08	12/3–12/20
Leap years	1/1–1/18	2/11–2/28	3/25–4/11	5/6–5/23	6/17–7/04	7/29–8/15	9/9–9/26	10/21–11/7	12/2–12/19

mesoscale details to the driving PCM, which are crucial to study the air quality conditions in SJV and SoCAB. Hourly averaged WRF outputs were calculated within the model and saved every hour for three-dimensional (3D) meteorological variables that can influence air pollution, such as wind, temperature, and humidity. Two-dimensional variables were also saved, including the aforementioned variables at the surface level, the mixing layer height, precipitation, etc. WRF performance was evaluated with these variables. In addition, the hourly averaged WRF outputs were used as the meteorological inputs for the University of California, Davis (UCD)–California Institute of Technology (CIT) air quality model (Kleeman and Cass 2001) in a different study (Mahmud et al. 2010, manuscript submitted to *Environ. Sci. Technol.*). It was necessary to simulate across a 7-yr period to account for the ENSO cycle that usually has a period of 6–8 years. Indeed, a major shortcoming of previous studies is that they fail to account for ENSO effects when simulating climate impacts on air pollution meteorology in California. Therefore, two 7-yr periods, 2000–06 and 2047–53, were chosen for present and future simulations. The dynamical downscaling approach at such fine resolution is computationally expensive. Therefore, to alleviate the computation burden while still supporting the calculation of annual average pollution concentrations— in the follow-up air quality studies (Mahmud et al. 2010, manuscript submitted to *Environ. Sci. Technol.*) without bias toward any season or time period—2 weeks out of every 6 weeks (as shown in Table 1) are used instead of the complete 21 years (i.e., 14 years with PCM data for the 2 time periods and 7 years with GFS data for the present time period). The first three days' simulations, which can be highly influenced by unrealistic, unbalanced flow in the initial conditions and the model spinup problem, were discarded; therefore, each simulation included 17 rather than 14 days. Because PCM only provides 28 days' simulation for February in leap years, 29 February was avoided by shifting simulation periods by one day for leap years, introducing an offset of one day from the normal year cases.

Simulations were also run using GFS reanalysis data for initial and lateral boundary conditions. GFS reanalysis data are available every six hours with a horizontal resolution of $1° \times 1°$, and have been widely used to drive regional climate simulations. This dataset assimilates many observations, including satellite data and conventional data, and, in general, is of good quality (Saha et al. 2006). Therefore, identical simulations were carried out using PCM or GFS reanalysis data for 2000–06 for comparison. The data bias of PCM can be estimated by comparing the climatology between these two global datasets; the extent to which this bias is propagated through to the downscaling results can be identified by driving simulations with both PCM and GFS data and comparing the results.

b. PCM model

PCM is a fully coupled GCM. It is composed of the National Center for Atmospheric Research (NCAR) Community Climate Model version 3 (CCM3), the Los Alamos National Laboratory Parallel Ocean Program (POP), the sea ice model from the Naval Postgraduate School, and a land surface biophysics model (Dai et al. 2004; Washington et al. 2000). The atmosphere component of PCM has a T42 horizontal resolution, which is approximately 2.8 degrees in latitude and longitude, and 18 vertical hybrid sigma-pressure levels. The ocean component of PCM has a higher resolution than most other GCMs near the equator, which leads to stronger El Niño signal and greater interannual tropical climate variability (Washington et al. 2000). PCM simulations can be conducted under different forcing scenarios. In this study, the atmospheric component of the BAU B06.44 simulation, which spans the period of 1995–2099, were used to provide initial and boundary conditions for WRF downscaling. The greenhouse gas concentration and SO_2 emissions applied in the BAU B06.44 scenario were described in Dai et al. (2001). The emissions for the two most important gases, CO_2 and SO_2, were generated using energy economics models, as the emissions of SO_2 are largely tied to the economic levels. The CO_2 level in year 2100 represents an approximate doubling of the level in year 2000 (Dai et al. 2004). The atmospheric, land, and sea ice conditions from a historical PCM simulation (case B06.28) were used to initialize the BAU B06.44 simulation, while the initial ocean conditions were derived from the assimilated ocean data (Dai et al. 2004; Pierce et al. 2004).

c. WRF model and the interface between WPS and PCM

WRF is a community mesoscale meteorology model, which is suitable for both operational forecasting and atmospheric research needs. The development of WRF has been a collaborative work among several research institutes. The Advanced Research WRF core (ARW) version 2.2 (Skamarock et al. 2007; Michalakes et al. 2001) was adopted in this study. The fluid in WRF ARW is treated as fully compressible and nonhydrostatic. WRF uses terrain-following vertical coordinates and the variables are horizontally staggered on an Arakawa C grid. The governing equations are written in flux form so that mass and dry entropy are conserved. The third-order Runge–Kutta scheme with time-splitting technique is used for temporal integration, and the third- and fifth-order advection schemes were chosen for the vertical and horizontal directions, respectively. Both idealized case and real case simulations are available in the WRF model.

WRF Preprocessing System (WPS), which reads in the global data and interpolates data to WRF grid points, could not process PCM data directly. Therefore, an interface program was developed to bridge PCM and WPS. The 3D variables, such as wind and temperature, were interpolated to 21 fixed pressure levels; the lowest level of these 3D variables and surface level properties were vertically interpolated to produce T2, 2-m humidity, and 10-m wind. For snow- and soil-related variables, PCM only provided daily data, which were used to derive 6-hourly data, under some assumptions, for WRF simulations.

d. *WRF basic configuration*

Three domains with two-way nesting were configured for the WRF simulations. The resolutions for domains 1–3 were 36, 12, and 4 km (Fig. 1b), respectively. The vertical direction had 31 stretched sigma levels with seven layers in the first kilometer and the model top extending to 50 hPa. The time step for domain 1 was 180 s. The finest resolution (4 km) domain (i.e., domain 3), which encompassed all of CA, provides the model's capability to capture mesoscale features under complex topography and intricate flow patterns in this area. To choose the most suitable physics parameters for this study, simulations for year 2000 with six different suites of physics schemes were examined and compared with observations, which will be described in the next section. To avoid the drifting of larger-scale features after long-term integration, four-dimensional data assimilation (FDDA) was applied to domain 1 using the driving global data (PCM or GFS) during the 17 days' integration. SST was updated every two days for domain 1. All analyses in this study used the simulation results from the innermost domain (i.e., the 4-km resolution one).

TABLE 2. Six suites of physics schemes tested for WRF simulations.

	Suite 1	Suite 2	Suite 3	Suite 4	Suite 5	Suite 6
PBL	YSU	YSU	MYJ	MYJ	YSU	MYJ
Cumu.	KF	Grell	KF	Grell	Grell	Grell
Micro.	Thomp.	Thomp.	Thomp.	Thomp.	WSM6	WSM6

3. Tests of different physics schemes in WRF

a. *Numerical experiments design*

Different physics schemes perform differently in WRF depending on the meteorological conditions and environment. In this section, six suites of physics schemes (Table 2), in combination with various planetary boundary layer (PBL) parameterizations, cumulus parameterizations, and microphysics, were tested for the whole year 2000 driven by GFS data. The temperature and moisture flux profiles in the boundary layer are primarily determined by the PBL parameterization, thus this physics component is crucial for the conditions within the boundary layer, where air pollution problems occur. Precipitation, which is mainly handled by the cumulus parameterization and microphysics, is another main factor affecting regional air quality as rainfall can scavenge airborne pollutants and modify low-level meteorology conditions through changes in soil moisture. GFS reanalysis data, rather than PCM data, were used for these simulations because GFS data are of higher quality owing to the assimilation of observations (Saha et al. 2006). As a result, the best model configuration selected from the simulations driven by GFS data is more reliable and more likely to reflect the actual WRF performance for our focus regions. The physics parameterizations evaluated were the following: for PBL, the Yonsei University (YSU) scheme (Hong et al. 2006) and the Mellor–Yamada–Janjic turbulent kinetic energy (TKE) scheme (MYJ) (Janjic 2002; Mellor and Yamada 1982); for cumulus parameterization, the Kain–Fritsch (KF) scheme (Kain 2004) and the Grell–Devenyi scheme (Grell and Devenyi 2002); and, for microphysics parameterization, the Thompson scheme (Thompson et al. 2004) and the WRF single moment 6-class (WSM6) parameterization (Hong et al. 2004). No cumulus parameterization was used for the third domain because of its fine resolution. All simulations used Rapid Radiation Transfer Model (RRTM) longwave (Mlawer et al. 1997) and Dudhia shortwave radiation (Dudhia 1989). The surface moisture fluxes are functions of the vegetation type and surface soil moisture in the thermal diffusion scheme. In CA, irrigation is a major source of soil moisture in spring and summertime. In WRF, the irrigation effect is implicitly included in the vegetation type (i.e., greenness) but not in the soil moisture (i.e., dry bias), which only

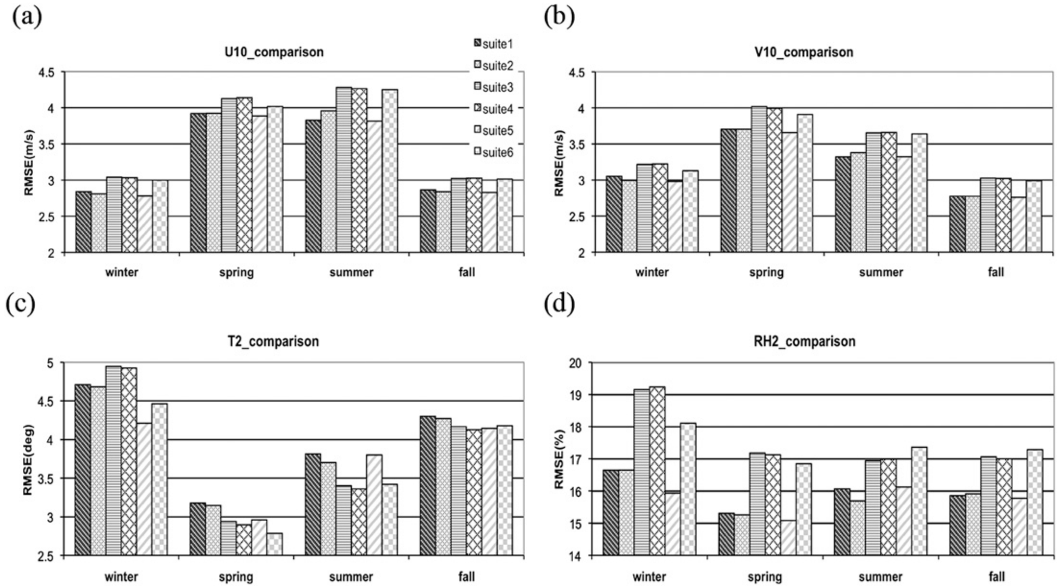

FIG. 2. Seasonal RMSE of model simulated (a) U10 and (b) V10, and (c) T2, and (d) RH2 with the six suites of physics schemes compared to observation data averaged over all stations in CA. The six suites defined in Table 2 are listed in order in the plots.

takes rainfall into account because of a lack of information on irrigation practices. However, the thermal diffusion scheme calculates moisture fluxes from vegetation greenness as estimated from satellite data with seasonal variation. Therefore, the greenness due to irrigation is implicitly included. Consequently, a 5-layer thermal diffusion scheme instead of a more sophisticated land surface model was used in the simulations to avoid underestimating moisture fluxes because of the dry-soil moisture bias (R. Fovell 2009, personal communication, from UCLA). Other model configurations were described in section 2. In the WRF simulations, each month was split into two runs. The first run included the first 15 days of the month, and the second run included the rest of the month. These simulations did not add an extra 3 days for model spinup to the integration period.

b. Results analysis

To evaluate WRF performance with the six physics suites, the simulation results from the third domain were compared with hourly observations collected from stations operated by the California Air Resource Board (CARB). During 2000, the year of the simulations, there were approximately 40 stations measuring surface temperature and humidity and 10 collecting surface wind data. Figure 2 shows the statewide-averaged seasonal root-mean-square error (RMSE) of WRF simulated results [10-m x-component wind (U10), 10-m y-component wind (V10), T2, and 2-m relative humidity (RH2)] calculated relative to observational data. In general, the wind error is larger in summertime than in wintertime, while the thermodynamic fields (e.g., temperature and moisture) show the opposite trend. Model performance with the different physics schemes was also evaluated with PBLH that was derived using the dry adiabatic lapse rate from Radio Acoustic Sounding System (RASS) observations available from 18 stations in CA during summer 2000 (Table 3). The model performed better for surface wind, relative humidity, and PBLH with the YSU PBL scheme (suites 1, 2, and 5). Suite 5 was best able to reproduce surface temperature in the winter but not the other three seasons.

Surface meteorology from the model simulations was further evaluated using the ''persistent score'' method: for each observed variable (e.g., T2), the suite with the best performance at each station for each time point was identified and given one point, while all other suites were given zero. The final score each suite received for each variable was divided by the total number of comparisons (i.e., the total number of records for each variable), giving the percent in which each suite was optimal for each variable (Fig. 3). This will help confirm the

TABLE 3. RMSE and bias of PBLH (m) from WRF simulations with six different suites of physics schemes during summer 2000.

	Suite 1	Suite 2	Suite 3	Suite 4	Suite 5	Suite 6
RMSE	445	449	830	828	444	830
BIAS	−82	−79	439	435	−84	437

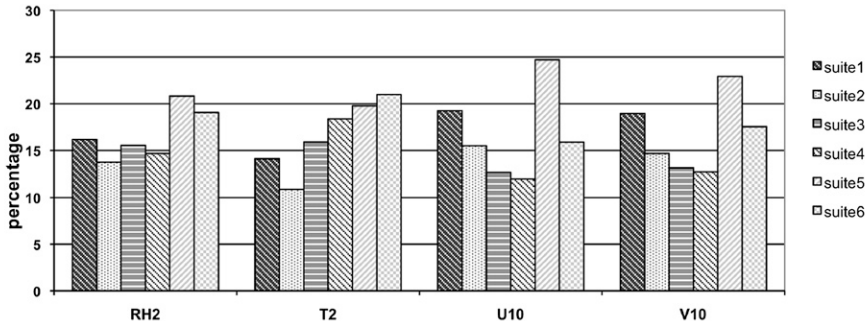

FIG. 3. Persistent scores: percentage of records for which each suite performed the best with respect to (left to right) RH2, T2, U10, and V10. The total counts for T2, RH2, and wind component comparisons are 55 833, 45 837, and 14 883, respectively. The six suites defined in Table 2 are listed in order in the plots.

relative performance (station-wise and time-wise) of the six suites. WRF configured with the physics schemes of suite 5 performed systematically better for relative humidity and surface wind, which are important variables for air pollution studies; however, it did not provide superior T2 results when evaluated by either method.

Analyses from both of the methods suggest that suite 5 is the best physics combination for CA. Simulated upper-air data, such as 500-mb winds and height, 850-mb temperature, and water vapor mixing ratio, were also compared to GFS reanalysis data using both comparison methods (plots not shown), and the same conclusion was obtained. Therefore, the physics schemes in suite 5 were applied for the main simulations in this study.

4. Downscaling results analysis

a. Downscaling results driven by PCM versus GFS data

After a 10-yr spinup time and 50-yr adjustment period, the fully coupled PCM integrated for about 100 years to establish the B06.44 BAU scenario data, which was used to drive WRF simulations in this study. There were no adjustments to match observations during the 100 years' PCM simulation. Therefore, there can be remarkable differences between PCM results and the National Center for Environmental Prediction (NCEP)'s GFS reanalysis data, as well as between the downscaling results driven by these two global datasets. GFS data were treated as unbiased to evaluate the PCM data and downscaling results, and the systematic errors (i.e., biases) of the WRF model were assumed to be consistent between both downscaling runs.

The dynamical downscaling procedure was described in section 2. Downscaled results driven by PCM data (called PCM WRF runs) were assessed with comparisons to the simulations with GFS data (called GFS WRF runs). Temperature is directly related to the greenhouse gas forcing scenario in the driving PCM simulations, and it is also an important factor for summertime ozone formation. Wind and PBLH determine the ventilation rate. Thus, the PCM WRF validation focused on these three variables. T2, wsp10, and PBLH of the downscaling results were averaged over 7 years (2000–06) for summer (simulation cases 5 and 6; see Table 1) and winter (simulation cases 1, 2, and 9). The analyses focused on these two seasons, which are when most ozone and PM problems occur in CA. The differences of the seasonal means of GFS WRF from PCM WRF were calculated and are shown in Fig. 4.

Figure 4a shows that, in summer, the PCM WRF downscaling results overestimated surface temperature over the Pacific Ocean, the coastal region (especially southern CA), and most of the San Francisco Bay Area but underestimated it inland. The magnitude of the under prediction is slightly smaller in the Central Valley than in other areas of CA. Land–sea temperature contrast is the most important factor in the formation of land–sea breeze, which is an evident phenomenon along the coastline and plays a large role in California's weather and air quality, especially during summer. Thus the comparison of PCM WRF and GFS WRF yielded disparate results over the coast region of CA and the adjacent ocean (Fig. 4a) suggests that these two sets of simulations predict dissimilar land–sea breezes. More details of land–sea breeze in CA and its future changes will be explored in Part II of the study (Zhao et al. 2011). During winter, PCM WRF simulations underestimated T2 for almost the entire analysis domain, except for over the Pacific Ocean adjacent to Southern CA and Mexico. The negative bias increased with distance inland and was as great as $-4°$ to $-5°$ in some regions.

There was a clear overestimation of surface wind speed (i.e., wsp10), by approximately 3 m s^{-1}, off the

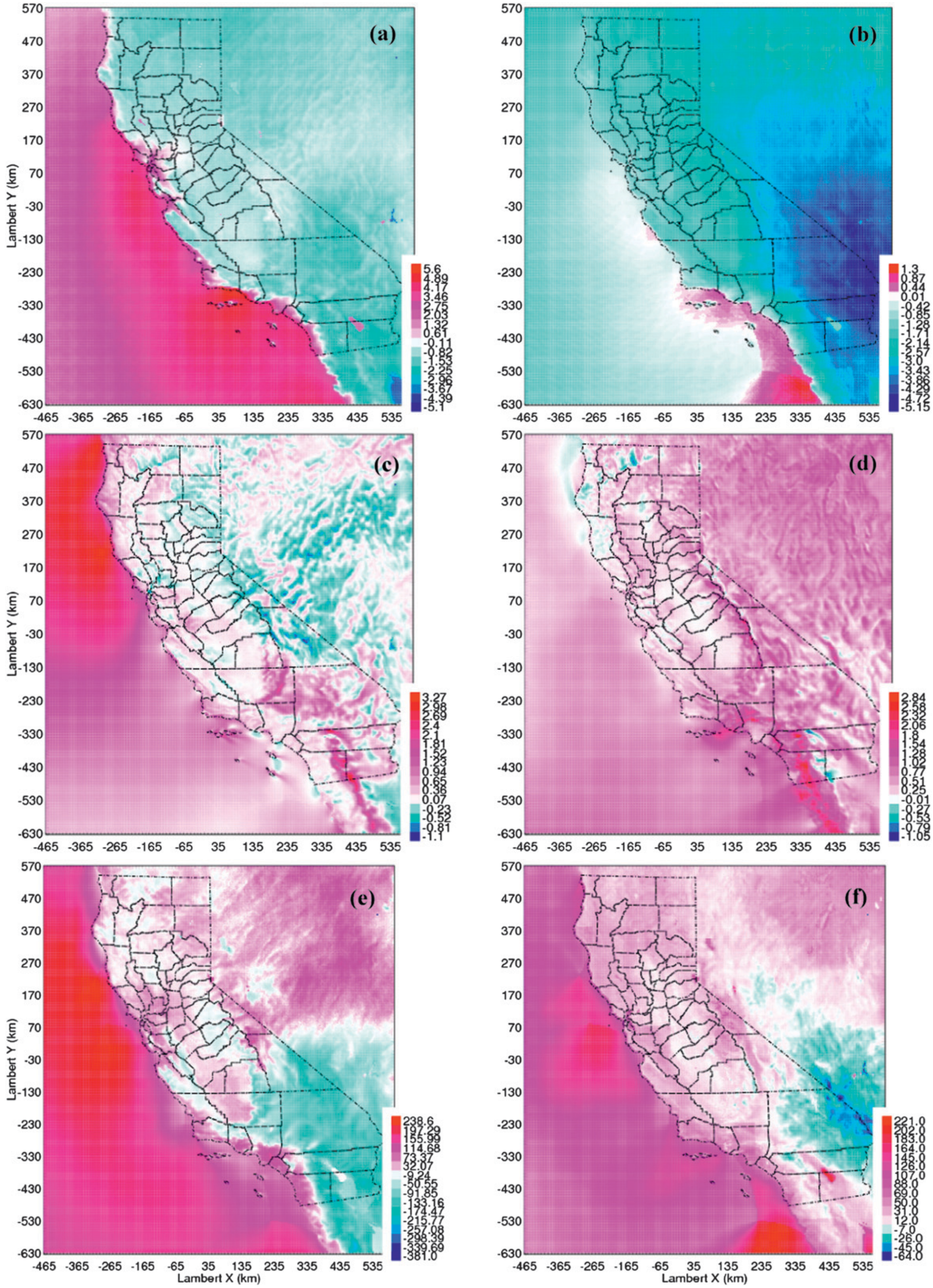

FIG. 4. Spatial distribution of differences between 7-yr-averaged WRF results driven by PCM and GFS data (PCM–WRF − GFS–WRF) for T2 (K) during (a) summer and (b) winter; wsp10 (m s^{-1}) during (c) summer and (d) winter; and PBLH (m) during (e) summer and (f) winter.

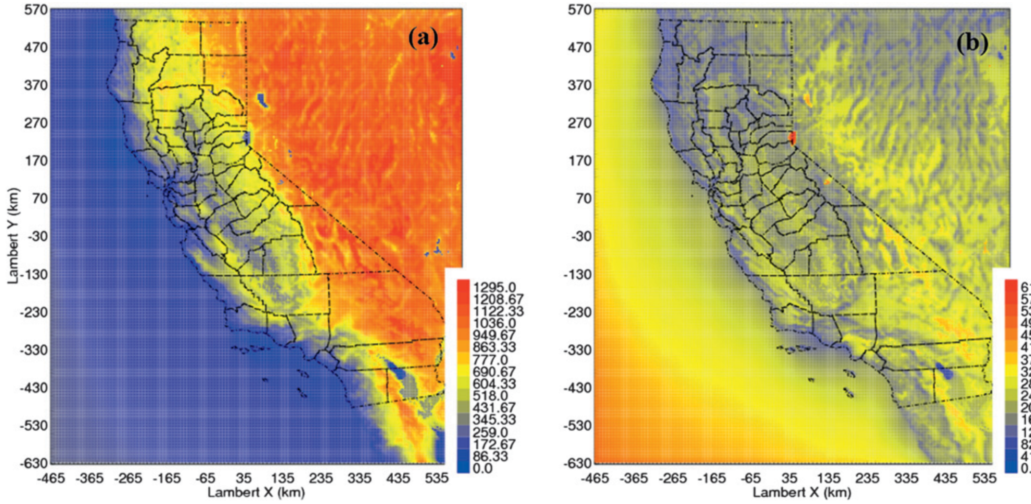

FIG. 5. The 7-yr-averaged PBLH from GFS WRF simulations during (a) summer and (b) winter. Units are in m.

coast of northern CA during summer (Fig. 4c). However, it must be borne in mind that the wind data in GFS reanalysis might not be of good quality, particularly over data sparse areas such as the ocean, owing to observational error. There were no significant wind speed differences in the Central Valley in the summer (Fig. 4c), but winds were slightly overestimated by PCM WRF in this region during winter (Fig. 4d). Wind speed was over predicted in much of SoCAB, particularly during winter. Note that the general overestimation of wind speed by PCM WRF is due to differences in the synoptic-scale pattern associated with the PSH in the original PCM and GFS global datasets, which is discussed later in this section. This synoptic wind difference dominates the wind speed comparisons and is much stronger than the expected weakening of the land–sea breeze by the weakened temperature gradient (Fig. 4a) over ocean and land in PCM WRF. Overall, the surface wind speed bias from PCM WRF simulations was more significant during winter than summer for the inland part of the analysis domain, despite the fact that surface wind is generally weaker in winter than in summer in CA.

The 7-yr-averaged PBLH downscaled in GFS WRF simulations was around 300–400 m in SJV and even lower in Los Angeles County (LAC) during summer (Fig. 5a). The former is due to the high pressure system and valley wind (see discussion in Section 4c), while the latter is due to a marine atmospheric boundary layer inversion (Singal et al. 1986). The wintertime average PBLH from GFS WRF simulations was about 200 m over SJV and SoCAB (Fig. 5b). The summertime PBLH bias (Fig. 4e) from PCM WRF was within 50 m in SJV; while in coastal (inland) SoCAB, the bias was around + (−) 100 m. The wintertime PCM WRF PBLH bias (Fig. 4f) was over 50 m for LAC and relatively small in other regions of SoCAB and SJV. Considering the low PBLH in these regions, the over predictions in LAC and SJV during both summer and winter were substantial, particularly in LAC.

Based on the above results, there were notable differences between PCM WRF and GFS WRF in reproducing meteorological fields closely related to air quality, which vary between regions and seasons. This may translate into differences in modeled seasonal average air pollutant concentrations, so it is essential to assess the impact of using atmospheric conditions from PCM WRF in air pollution studies. To do so, we consider the integrated effect of differences in these meteorological fields on air quality, again, assuming that the real atmospheric conditions are well reproduced by GFS WRF. Table 4 summarizes the integrated assessment in three regions of interest [i.e., SJV, coastal region of LAC (CLAC), and SoCAB other than CLAC (SoCABo)] during summer and winter. T2 is only considered in summertime when ozone is the primary pollutant in CA.

TABLE 4. Integrated assessment of PCM WRF performance compared to GFS WRF for WSP10, PBLH, and T2 and inferred effects on estimated air pollutant concentration (AQ) in SJV, coastal region of LAC (CLAC), and SoCAB other than CLAC (SoCABo) during summer and winter. The letter O indicates an overprediction, U an underprediction, and the minus sign (−) an unclear effect.

	Summer				Winter		
Region	WSP10	PBLH	T2	AQ	WSP10	PBLH	AQ
SJV	−	O	U	U	O	O	U
CLAC	O	O	−	U	O	O	U
SoCABo	O	U	U	−	O	O	U

Note that these meteorological fields affect air pollutant concentration simultaneously and nonlinearly. It is very likely that the wintertime air pollution problem in all three regions will be underestimated with atmospheric conditions from PCM WRF. The net effect on estimated summertime air quality is difficult to appraise owing to the addition of T2. Summertime pollutant concentration in SJV may be under predicted owing to overestimates of PBLH and underestimates of T2 from PCM WRF. It is relatively difficult to infer the effect of PCM WRM biases in SoCABo, but air pollution problems are likely to be underestimated in these regions, particularly in LAC. The influences of PCM WRF on estimating extreme air pollution events, which normally happen during atmospheric stagnation, are discussed in Part II of this study (Zhao et al. 2011). There we show that in SJV both the total number of stagnant days and the strength of the stagnation were underestimated by PCM WRF during summer and winter; therefore, extreme air pollution events are also likely to be under predicted with fields from PCM WRF.

To investigate the sources of the differences between the two sets of simulations, the climatology from the original PCM and GFS data for a much larger region were analyzed. GFS data were averaged to the horizontal resolution of the PCM data to facilitate the comparison. In the summertime, the PSH in PCM (Fig. 6a) data was stronger and farther north. Consequently, PCM also had a stronger pressure gradient, which may partially explain the higher wsp10 present off the coast of northern CA in the PCM WRF results (Fig. 4c). The more northerly location of the PSH in PCM, in combination with the coast mountain range in Canada, blocked cold air in Canada from moving south (Fig. 6a). In contrast, in GFS more cold air intruded to the south and dominated larger areas of inland CA and the adjacent Pacific Ocean (Fig. 6b). This explains the positive T2 difference between the downscaling results driven by PCM and GFS data over the Pacific Ocean during summer (Fig. 4a). In contrast, the under prediction of inland T2 by PCM WRF (Fig. 4a) was not present in the original PCM data (Fig. 6e), thus it was generated by the downscaling process. Another feature shown in Fig. 6 is that the North American Thermal Low (NATL) was well developed in PCM data during summer but not in GFS (Fig. 6a versus 6b). Figure 7 shows the averaged 500-mb geopotential height from PCM and GFS data in summer. There was a trough located above the west coast in both models. However, the pressure gradient upstream of the trough was stronger in PCM data. This may be what caused the PSH in PCM to be stronger and farther north (i.e., a stronger wind for a stronger negative vorticity advection). Note that the wind vectors around the PSH in Fig. 6 do not represent the real wind field. The movement of the PSH causes substantial changes in the wind field in parts of the domain, and therefore both the wind speed and wind direction are cancelled out considerably in the calculation of seasonal averages.

PCM data and downscaling results (Figs. 4a and 6e) have obvious similarities over the Pacific Ocean adjacent to CA, with biases in T2 of up to 4°–5° in both. PCM data had a small warm bias (approximately 1°–2°) for inland CA, while the downscaling results had small cold bias (approximately $-1°$). Possible reasons are that 1) the complex topography in CA might introduce extra error when interpolating coarse global data close to the surface for input to fine resolution WRF simulations; and 2) the summer means were averaged over cases 5 (18 June–5 July) and 6 (30 July–16 August) for the downscaling results, but over the whole 3 months (June, July, and August) for PCM data, so some discrepancy between the two is expected.

Compared to summertime, the wintertime climatology patterns from PCM (Fig. 6c) and GFS (Fig. 6d) data were more similar. This might be due to stronger signals in wintertime (e.g., the baroclinic zone). However, it is noted that the high pressure system over the western United States was well formed and elongated to the northwest–southeast from PCM. This helped transport cold air more efficiently southward from southern Canada and the northern United States. As a result, strong cold T2 anomalies between PCM data and GFS occurred in Texas and Arizona (Fig. 6f), and this was carried over to southeastern CA through downscaling (Fig. 4b).

Overall, the strength and position of the PSH, which determines the amount and pattern of cold air in Canada intruding south, played an important role in the difference between PCM and GFS data in summer. Thermal lows (highs) in summer (winter) over the western United States also contributed to the difference between these two global models, to some extent. PCM bias corrections will be needed to improve the downscaling results.

b. Surface comparison between simulation results and observational data

To evaluate the model performance, the simulation results were compared with aviation routine weather report (METAR) surface weather observational data, which were available every hour at 66 stations in SoCAB and 12 stations in SJV during the 2000–06 period. In METAR data, surface wind speed (i.e., wsp10) and temperature (i.e., T2) are recorded for the two minutes prior to observation time and averaged. By comparing to observational data, simulation errors internal to the WRF model can be explored for these specific areas and model configuration. Unsurprisingly, the simulations driven

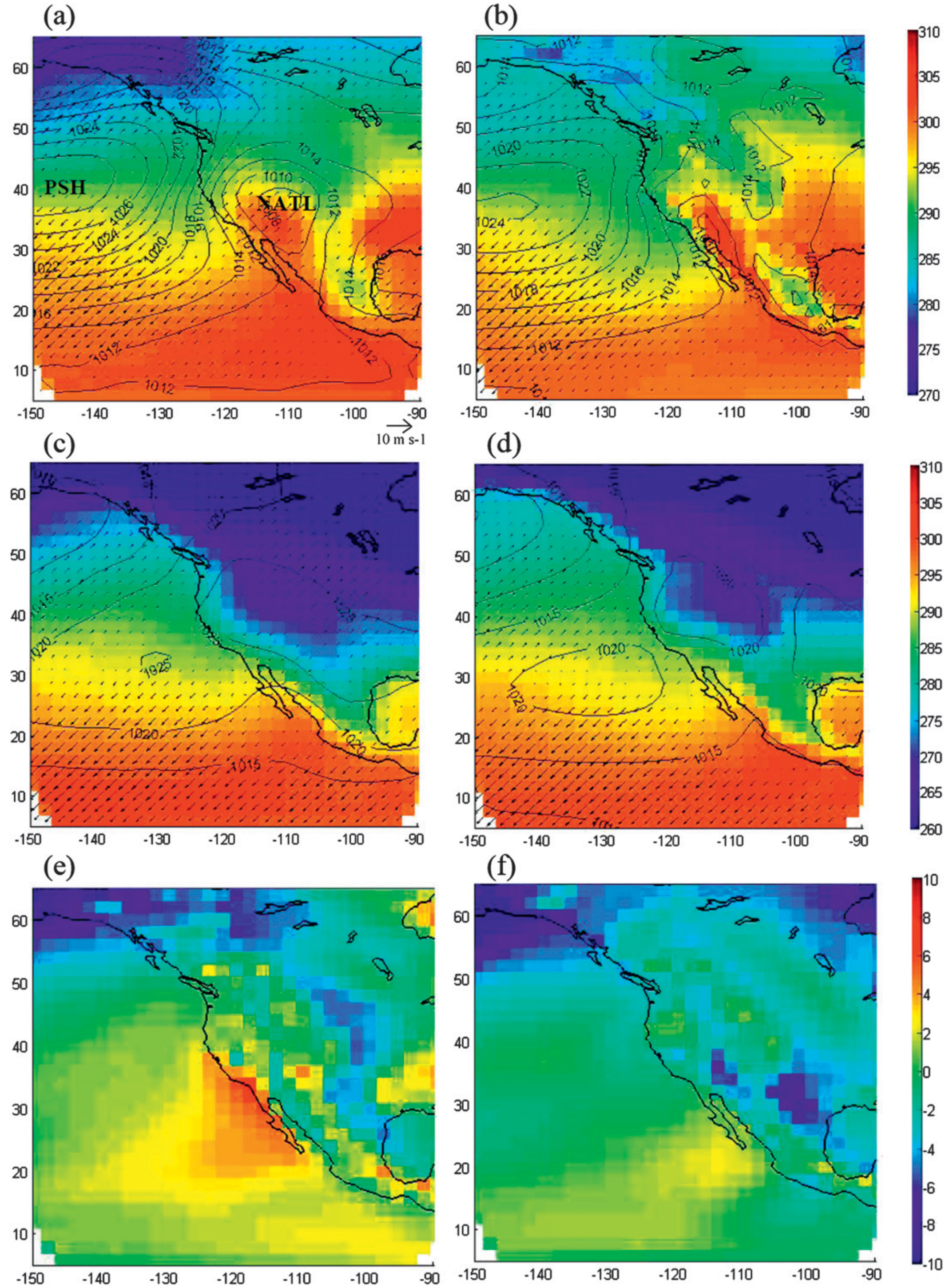

FIG. 6. Spatial distribution of 7-yr-averaged T2 (shading, K), sea level pressure (contour lines, mb), and wind vectors of (a) PCM data for summer, (b) GFS data for summer, (c) PCM data for winter, (d) GFS data for winter; and T2 difference between PCM data and GFS data (PCM − GFS) for (e) summer and (f) winter.

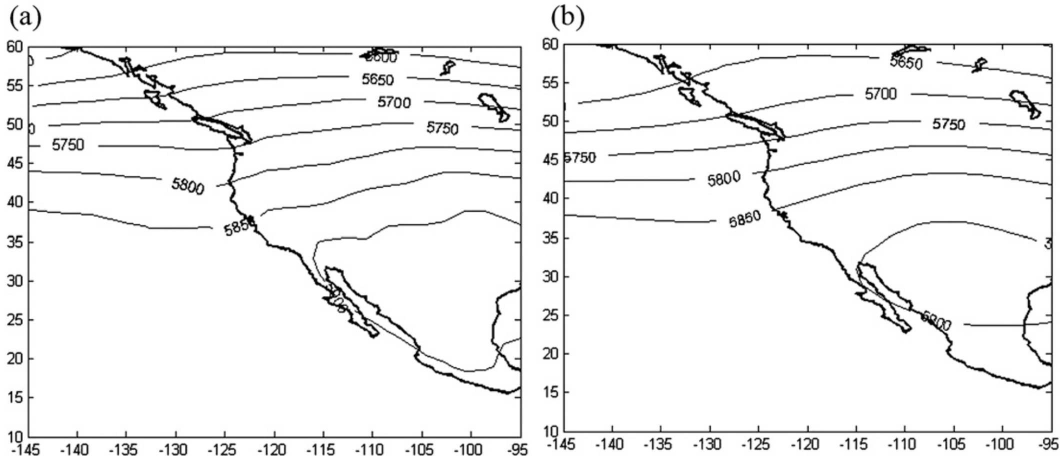

FIG. 7. The 7-yr-averaged 500-mb geopotential height of (a) PCM and (b) GFS data during summer. Units are in m.

by GFS data generally matched the observations better than their counterparts with PCM data. Figure 8 shows the T2 bias of the simulations driven by GFS (dark gray) and PCM (light gray) data averaged over time (the 7 years simulated) and space (the METAR stations) in SoCAB (Fig. 8a) and SJV (Fig. 8b). Simulations with GFS data overestimated T2 for both SoCAB and SJV. GFS WRF performed better during summer than winter, and the wintertime simulation was better in SoCAB than SJV. Poorer performance may be associated with a temperature inversion, which happens during winter and is stronger in SJV than SoCAB. WRF is known to have difficulty reproducing conditions within the shallow boundary layer associated with these temperature inversions. PCM WRF overestimated T2 largely during fall (cases 7 and 8). The bias comparisons between simulations with the two global datasets are consistent with Figs. 4a and 4b, which show that the simulations with PCM data predicted lower T2 over land during summer and winter. The general $\sim(-2$ to $+2$ K) bias of T2 from GFS WRF simulations suggests that WRF performance is acceptable considering the complex topography and mesoscale flow patterns in CA. The downscaling results with PCM data had an exceptionally warm bias for case 7, which spans 9–26 September, in both regions. Figure 9 compares T2 from PCM and GFS during this time. The overall systems were in accord with those during summer (Figs. 6a and 6b), but the PSH weakened in both of the global datasets during fall. The PSH in GFS data helped to bring the cold air in Canada to the western United States. In contrast, the PSH in PCM data was elongated to the northeast relative to its position in the summer (Fig. 6a), constraining the cold air to latitudes above 45°N. Consequently, the surface temperatures were quite different between the two global datasets as well as their downscaled simulation results in CA for this case (i.e., case 7).

Figure 10 shows the wsp10 bias of each simulation case averaged over the 7-yr study period relative to METAR observations. Both simulations overestimated wsp10 for most cases. Much greater overestimation occurred in the simulation with PCM data in SoCAB during winter (cases 1, 8, and 9), as was also apparent in comparisons of PCM WRF with GFS WRF (Fig. 4d).

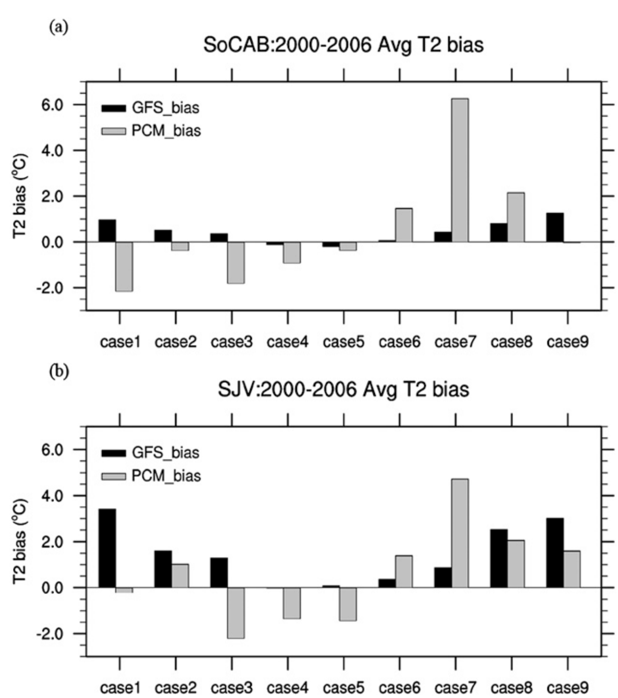

FIG. 8. The 7-yr-averaged T2 bias (K) over (a) SoCAB and (b) SJV for each simulation case driven by GFS and PCM data.

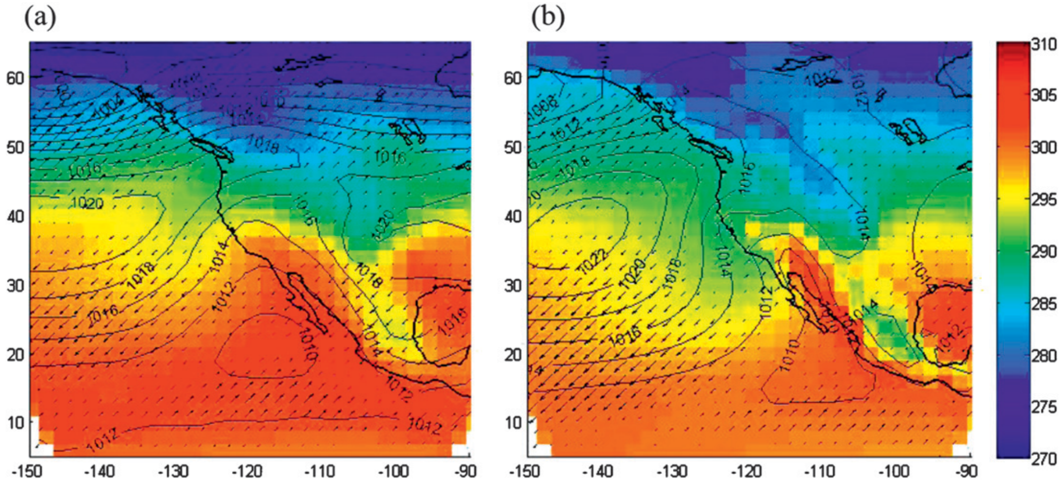

FIG. 9. As in Fig. 6, but for case 7.

The smaller magnitude of bias in SJV could be due to SJV having weaker wind overall than SoCAB. In terms of bias, WRF generally simulated wsp10 better in summer than winter, though both seasons are known to have relatively calm wind owing to the influence of the PSH moving inland. However, in addition to bias, discrepancies between model results and observations may have arisen because sparsely distributed surface observations were compared to a uniformly spaced, 4-km model grid, as well as from the inherent uncertainty of wind observations in general. Note that the seasonal trends of model performance in simulating wsp10 are the opposite in terms of RMSE (Fig. 2) and bias (Fig. 10). The larger RMSE but smaller bias in the summer can occur if model simulations have a larger uncertainty but the errors have opposite signs and thus cancel each other out. Another explanation is that only year 2000 was simulated to test the six physics suites (Fig. 2), while the simulation period for the results described in this section (Fig. 10) was 2000 ~ 2006.

Wind direction was not validated in this study, however, using PCM WRF results, Mahmud et al. (2010) show that the UCD–CIT air quality model successfully predicted the spatial pattern of $PM_{2.5}$ concentrations in CA, which suggests that the wind directions from WRF simulations are generally reasonable. However, the annual average concentrations of $PM_{2.5}$ were underpredicted by the UCD–CIT air quality model by ~(35–40)% (Mahmud et al. 2010). Generally speaking, high $PM_{2.5}$ episodes in SJV and SoCAB occur during stagnant events, when winds are very weak. Previous studies have shown that WRF has difficulties in capturing the strength of stagnant events and the accompanying weak surface wind (Mölders and Kramm 2009; Zhang et al. 2009). A possible reason is that the vertical resolution may not be high enough to accurately resolve the wind within the low boundary layer during the stagnation events. To explore the possibility of this problem in our simulations, the model bias and RMSE were calculated with respect to the observed surface wind speeds. The observed wind speed has discrete values owing to the 0.5 m s^{-1} precision of METAR observational data. Similar results were found in both SoCAB and SJV, thus only the results for SoCAB are shown (Fig. 11). Over 80% of the observed wsp10 were under 5 m s^{-1}, which is why the range of

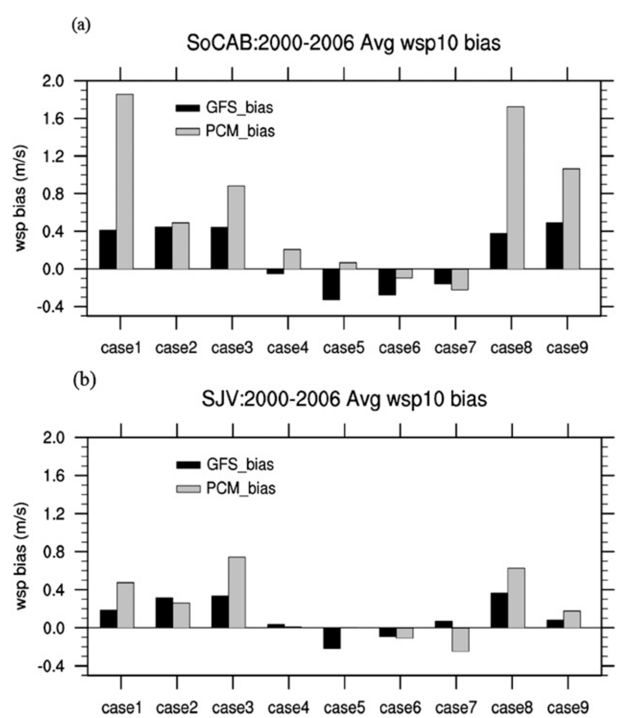

FIG. 10. As in Fig. 8, but for wsp10.

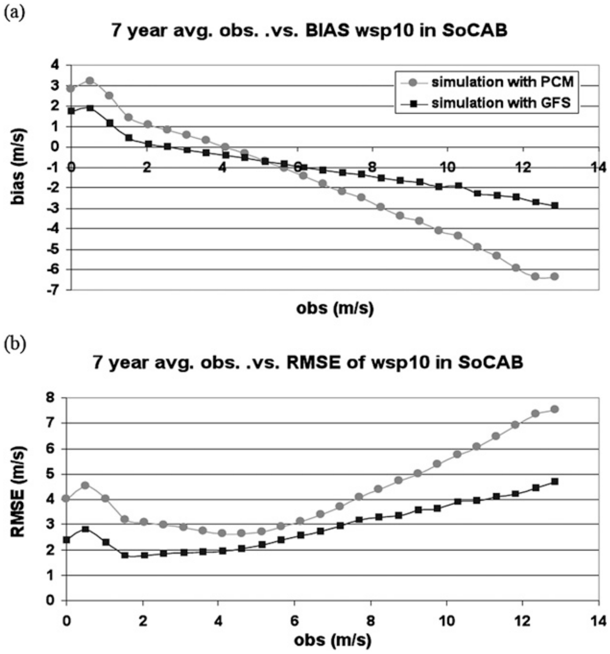

FIG. 11. The 7-yr-averaged model (a) bias and (b) RMSE with respect to observed wind speed in SoCAB.

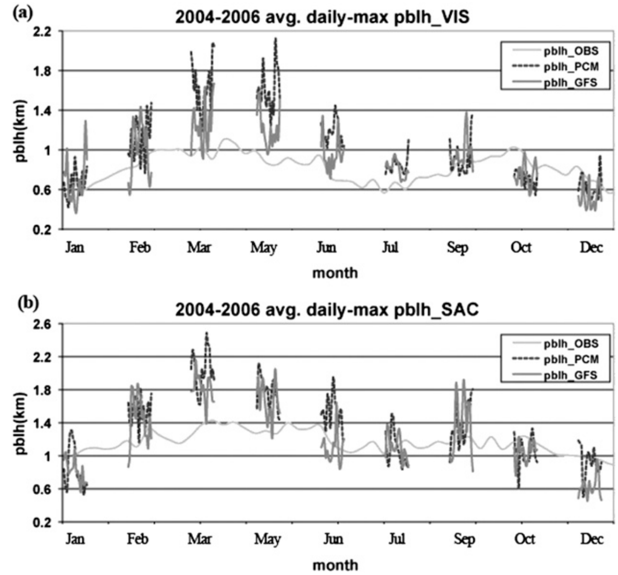

FIG. 12. The 3-yr-averaged (2004–06) daily maximum PBLH from observations (light gray solid line), PCM WRF simulations (dark gray dashed line), and GFS WRF simulations (dark gray solid line) at stations (a) VIS and (b) SAC.

the errors shown in Fig. 10a are quite different from those in Fig. 11a. It is obvious that for very calm wind ($\leq$1.5 m s^{-1}), WRF simulations with both datasets had a relatively large bias and high RMSE. Taking into account the small values of the corresponding wind speed observations, these biases and RMSEs are even more substantial. PCM WRF results also had relatively large bias (underestimated) and high RMSE for high winds. The difficulty of simulating weak surface wind may be a nonnegligible problem when applying the WRF model to provide meteorological inputs for air quality simulations, and it must be improved to capture air pollution episodes. Potential solutions, such as increasing the vertical resolution within the boundary layer or increasing the surface roughness, have been suggested and tested within the WRF community.

The analyses in this section showed that, in GFS WRF runs, T2 was overestimated and wsp10 was, in general, substantially overestimated in calm wind conditions and underestimated in high wind conditions. WRF performance was better during summer than other seasons. These patterns very likely represent the WRF systemic error (i.e., bias) in this region.

c. *Low PBLH during summer*

As PBLH is one of the most important meteorological inputs to air quality model simulations, additional investigations were carried out on this variable. As mentioned in section 4a, the 7-yr-averaged summer PBLH was about 300–400 m in the Central Valley. Yet, at the same latitude in Nevada, the PBLH was over 1000 m (Fig. 5a) despite the fact that T2 is higher in the Central Valley than Nevada (by over 3 K; figure not shown). In general, the high surface temperature (i.e., T2) overland during summer could promote vertical convection, which results in high summer PBLH. The possible reasons for the low summer PBLH in the Central Valley are explored in this section.

Figure 12 shows the 3-yr-averaged (2004–06) daily maximum PBLH from observational data, PCM WRF, and GFS WRF simulations at stations Visalia Airport (VIS) (36.30°N, −119.40°W) and SMAQMD_WP1 (SAC) (38.20°N, −121.30°W); the locations of both stations are shown in Fig. 1b. Only three-years of data are analyzed owing to the availability of the observations. The pblh_OBS shown in Fig. 12 are the 7-day-averaged daily maximum PBLH calculated from RASS observations. Averages were calculated to smooth small variations in the original observational data and better perceive the seasonal pattern. Summertime PBLH was also shallow in pblh_OBS (Fig. 12). Modeled PBLH were quite consistent from both global datasets, and they were in good agreement with observations. Overestimation occurred over both stations during springtime. GFS WRF generally predicted lower PBLH than PCM WRF did for most of the year. Overall, Fig. 12 shows that both PCM and GFS WRF simulations well captured the seasonal trend of the PBLH over the two stations in the Central

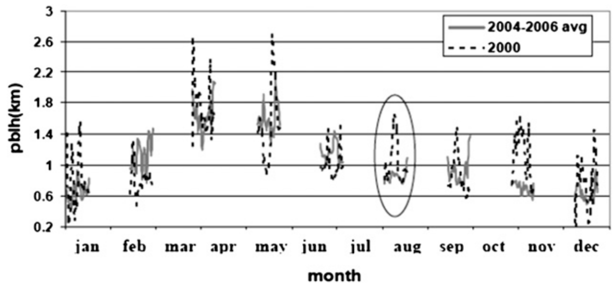

FIG. 13. The SJV-averaged daily maximum PBLH, averaged over 2004–06 (gray solid line) and during 2000 (black dashed line). The encircled part is from case 6.

Valley, and the shallow summer PBLH was present in the observations.

Analyses of stagnant events over SJV, the details of which are provided in Part II (Zhao et al. 2011) of this study, revealed that the PSH moved inland and dominated SJV for the majority of case 6 (30 July–16 August) during 2004–06 but only appeared for six days during 2000. The high pressure system over SJV always results in stagnant events featuring calm surface wind, low PBLH, etc. PBLH (from PCM WRF simulations) averaged over SJV from 2004–06 are compared to those from 2000 in Fig. 13. It is obvious that without the dominance of a high pressure system, the PBLH for case 6 (circled in Fig. 13) in 2000 was much higher. Therefore, the high pressure system is one cause of the low summertime PBLH in SJV.

Yet, even without a persistent high pressure system in 2000, the PBLH during summer was still only about half of that in springtime. This low PBLH is also caused by seasonal changes in the flow patterns in SJV. The boundary layer structure in a valley can be very complicated and vary temporally owing to cross-valley flow. SJV is a relatively wide valley, with an average valley floor width of 125 km and a depth of about 1 km on the west and over 3 km on the east side; consequently, the flow pattern and the PBL structure in SJV can be very different from the conceptual model of the convective boundary layer in deep valleys (Whiteman 1982; De Wekker et al. 2005; Kuwagata and Kimura 1997). Figure 14 shows the vertical cross sections of vertical wind velocity and potential temperature along an east–west gradient containing VIS (see Fig. 1b) at 1600 local time (LT) on 7 August 2000 and 28 March 2000. These dates were chosen to represent the flow patterns that normally appear in the afternoon during summer and spring in SJV, when the high pressure system is absent. The time of 1600 LT was selected as the WRF outputs were only saved four times a day (0400, 1000, 1600, and 2200 Pacific daylight time); among these times, PBLH is highest at 1600 LT, when the sun is facing the west side of the mountains. In summer, the valley wind was strong

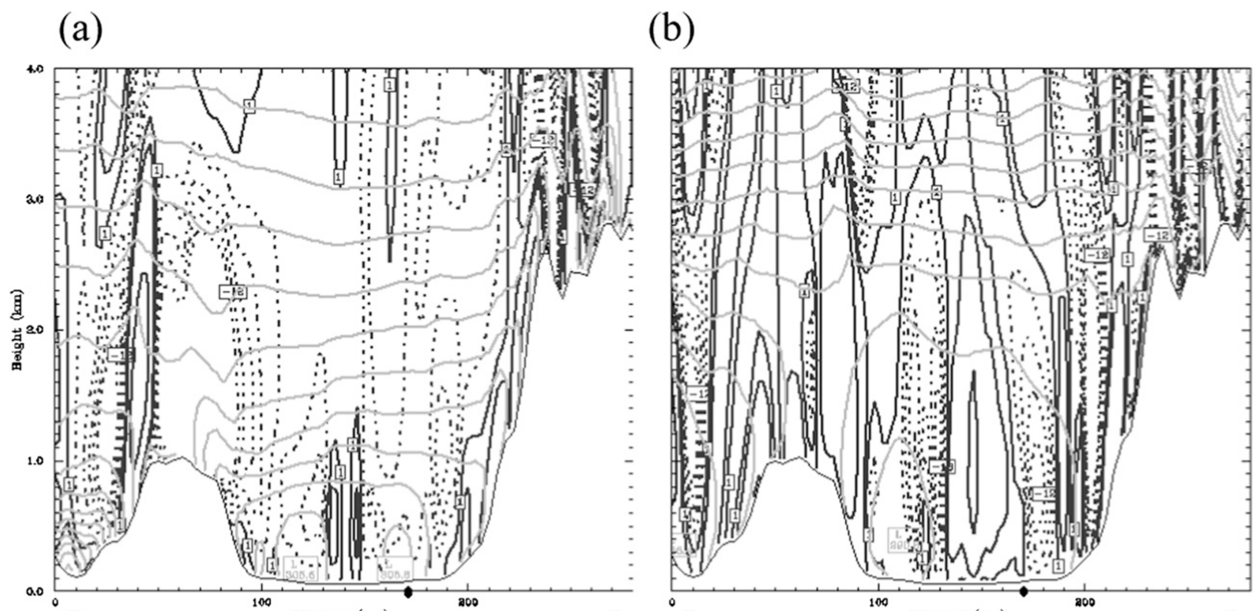

FIG. 14. Vertical cross sections of positive w (black solid lines), negative w (black-dashed lines), and potential temperature (gray solid lines) at 1600 LT on (a) 7 Aug 2000 and (b) 28 Mar 2000 along an east–west transect (shown in Fig. 1b) containing VIS (shown as black dot on x axis). The interval of the potential temperature and negative wind velocity in the plots is 1 K and 0.03 m s^{-1}, respectively. A contour interval multiplier of 3 (i.e., 1, 3, 9 cm s^{-1}, etc.) was applied to the positive wind velocity due to the strong upward motion in the mountain region.

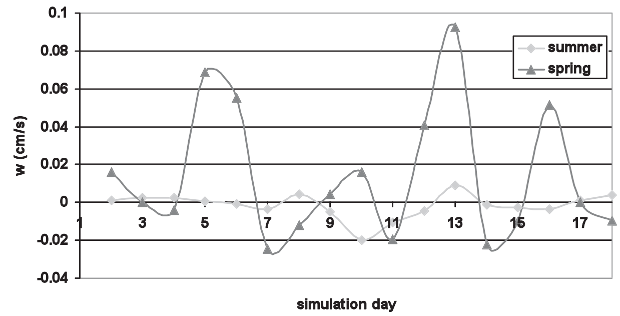

FIG. 15. The SJV-averaged 3-km vertical velocity at 1600 during simulation case 6 (summer) and case 3 (spring).

owing to strong differential heating (Fig. 14a). The associated downward flow, which appeared most places between the two mountain ranges, suppressed vertical convection near the surface and led to a very shallow PBLH over the Central Valley. In contrast, during spring, the valley wind signal weakened, and upward motion was much stronger and present at more places between the two mountain ranges than during summer. Note that VIS (the dot in Fig. 14) is located almost inside an upward motion area in springtime (Fig. 14b), and the PBLH might be higher there than other places in the valley for this particular case (i.e., case 3 in 2000). Nevertheless, the averaged PBLH in the Central Valley in the summertime was much shallower than that in the springtime, as indicated in the potential temperature field in Fig. 14.

The SJV averaged 3-km vertical wind velocity at 1600 LT was calculated from PCM WRF simulations for year 2000. Figure 15 shows the time evolution of the regional averages during case 6 (summer) and case 3 (spring). The negative values ($w < 0$) during case 3 occurred at the time of high pressure system dominance in the Central Valley. Upward motion ($w > 0$) was obvious for other simulation times because of solar heating over the Central Valley during spring. Weak subsidence occurred in the Central Valley for most of case 6 because of the dominance of the valley wind. Figure 15 indicates the overall summertime (springtime) downward or near zero (upward) motion above the boundary layer, which was below 3 km for all cases simulated during 2000 (Fig. 13) over SJV. Therefore, during the summer, the vertical convection within the boundary layer was suppressed by the valley wind above and resulted in low PBLH.

5. Conclusions and remarks

This study investigates the impacts of climate change on meteorology and air quality conditions in CA using the WRF model to dynamically downscale PCM data to high-resolution (4 km) simulations. As the first stage of the study, this paper focused on the downscaling results for the present climatology (2000–06) with two different datasets: PCM and GFS data. Comparing these two sets of simulations can determine the error due to PCM bias in the downscaling results. In addition, the WRF simulation results were evaluated against observational data.

The spatial distributions of PBLH, T2, and wsp10 during summer and winter were analyzed for the two simulations. When driven by PCM data, T2 was underestimated for most of the analysis domain during winter, while the underestimation mainly occurred inland during summer. Similar patterns were observed when comparing temperature from the original PCM and GFS data, which indicates that the downscaling biases are inherited from the driving PCM. However, for inland CA the sign of the bias between the original global data and the downscaling results were the opposite, as a result of the downscaling process. An imprecise prediction of the location and strength of the PSH, and consequently the pattern and amount of cold air intruding to CA from Canada and the northeastern Pacific Ocean are the main sources of the PCM data bias. PCM WRF overestimated wsp10 in CA and over the neighboring Pacific Ocean. With respect to the two regions with serious air pollution problems, the wsp10 overestimation was more obvious in SoCAB, especially during winter. PBLH was also overestimated for most regions in CA. T2, wsp10, and PBLH are the three most important meteorological factors affecting regional air quality. The bias of the downscaling results driven by PCM data imply that using these results as inputs for air quality models will probably underestimate the seasonal (i.e., summer and winter) pollutant concentration in CA, particularly in LAC.

The downscaling results were compared to surface observational data as well. The model bias of T2 and wsp10 were averaged over SJV and SoCAB for each simulation case. In general, WRF-simulated T2 matched the observations quite well, with a positive bias of less than 2 K. The temperature simulation was better during summer than winter, in terms of bias, and better for SoCAB than SJV. These statistics averaged over the two geographic regions were consistent with the spatial distribution analysis of the two sets of simulations. WRF overestimated wsp10 in these two regions. The evaluation of model bias–RMSE versus observed wsp10 showed that WRF has difficulty reproducing weak surface wind in these regions. It is crucial to solve this problem to have accurate air quality predictions using WRF simulation results as the meteorological inputs. Driven by the present 7-yr (2000–06) PCM WRF results, an air quality model successfully predicted the spatial distribution of $PM_{2.5}$ concentration in CA; nevertheless, the annual average $PM_{2.5}$ concentration were underestimated by about 35%–40% at different locations in SJV and SoCAB (Mahmud et al. 2010).

The spatial distribution of simulated PBLH reveals that the summertime PBLH is much lower in SJV compared to other inland regions at the same latitude. Two possible reasons are the dominance of a high pressure system and the strong valley wind in the daytime during summer over SJV; both of which provide downward motion above the boundary layer and suppress vertical mixing in this region.

This paper illustrates that the downscaling results inherit the biases of the driving GCMs through the lateral boundary conditions, which agrees with previous studies. To improve the performance of WRF downscaling, an ensemble of GCMs (CCSM3 and HadCM3, for instance) or PCM bias corrections will be required, which we leave for future work.

RCMs are widely used to dynamically downscale coarse-resolution GCM simulation results to higher resolution but there are several potential problems associated with this approach. Inconsistencies between GCMs and RCMs, such as different soil/vegetation information, numerical methods, physics parameterizations, etc., might produce a mathematically and physically ill-posed problem. In addition, meteorological variables within the boundary layer can be sensitive to the vertical and horizontal resolutions employed during the downscaling exercises. Finally, wind fields simulated over California, in particular the coastal region, are very sensitive to the strength and location of the PSH system, which can be influenced by the total domain size employed by the RCM. In this study, differences in synoptic-scale patterns were observed between WRF predictions and the driving global data. These differences could reflect real phenomena that are caused by interactions between the large-scale and small-scale systems, or these differences could be artifacts caused by inconsistencies between WRF and the original GCM. Further study is needed to fully identify best practices that avoid potential artifacts.

Acknowledgments. This research is supported by the California Air Resources Board (CARB) under Contract 04-349. We gratefully acknowledge the U.S. Department of Energy's (DOE) Office of Science (BER) Accelerated Climate Prediction Initiative (ACPI) project for supplying model simulations. We thank Stephen Zelinka from CARB and Sonoma Technology Inc. for providing us observational data. Thanks also go to the National Typhoon and Flood Research Institute and National Central University, Taiwan, which provided computer clusters for part of the model simulations, Kemal Gurer from CARB and Dr. Jian-Wen Bao at NOAA are thanked for help in the early stage of this study.

REFERENCES

Barnett, T. P., D. W. Pierce, and R. Schnur, 2001: Detection of anthropogenic climate change in the world's oceans. *Science,* **292,** 270–274.

Bell, J. L., L. C. Sloan, and M. A. Snyder, 2004: Regional changes in extreme climatic events: A future climate scenario. *J. Climate,* **17,** 81–87.

Caldwell, P., H. N. S. Chin, D. C. Bader, and G. Bala, 2009: Evaluation of a WRF dynamical downscaling simulation over California. *Climate Change,* **95,** 499–521.

Dai, A., T. M. L. Wigley, B. A. Boville, J. T. Kiehl, and L. E. Buja, 2001: Climates of the 20th and 21st centuries simulated by the NCAR Climate System Model. *J. Climate,* **14,** 485–519.

——, W. M. Washington, G. A. Meehl, T. W. Bettge, and W. G. Strand, 2004: The ACPI climate change simulations. *Climatic Change,* **62,** 29–43.

De Wekker, S., D. G. Steyn, J. D. Fast, M. W. Rotach, and S. Zhong, 2005: The performance of RAMS in representing the convective boundary layer structure in a very steep valley. *Environ. Fluid Mech.,* **5,** 35–62.

Dudhia, J., 1989: Numerical study of convection observed during the winter monsoon experiment using a mesoscale two-dimensional model. *J. Atmos. Sci.,* **46,** 3077–3107.

Duffy, P. B., and Coauthors, 2006: Simulations of present and future climates in the western United States with four nested regional climate models. *J. Climate,* **19,** 873–895.

Grell, G. A., and D. Devenyi, 2002: A generalized approach to parameterizing convection combining ensemble and data assimilation techniques. *Geophys. Res. Lett.,* **29,** 1693, doi:10.1029/2002GL015311.

Hay, L. E., and M. P. Clark, 2003: Use of statistically and dynamically downscaled atmospheric model output for hydrologic simulations in three mountainous basins in the western United States. *J. Hydrol.,* **282,** 56–75.

Hong, S.-Y., J. Dudhia, and S.-H. Chen, 2004: A revised approach to ice microphysical processes for the bulk parameterization of clouds and precipitation. *Mon. Wea. Rev.,* **132,** 103–120.

——, Y. Noh, and J. Dudhia, 2006: A new vertical diffusion package with an explicit treatment of entrainment processes. *Mon. Wea. Rev.,* **134,** 2318–2341.

Howard, C., A. Kumar, I. Malkina, P. Green, R. Flocchini, and M. J. Kleeman, 2010: Reactive organic gas emissions from livestock feed contribute significantly to ozone production in central California. *Environ. Sci. Technol.,* **44,** 2309–2314.

Jacobson, M. Z., 2008: Short-term effects of agriculture on air pollution and climate in California. *J. Geophys. Res.,* **113,** D23101, doi:10.1029/2008JD010689.

——, 2010: The enhancement of local air pollution by urban CO_2 domes. *Environ. Sci. Technol.,* **44,** 2497–2502, doi:10.1021/es903018m.

Janjic, Z. I., 2002: Nonsingular implementation of the Mellor–Yamada Level 2.5 scheme in the NCEP Meso model. NCEP Office Note 437, 61 pp.

Kain, J. S., 2004: The Kain–Fritsch convective parameterization: An update. *J. Appl. Meteor.,* **43,** 170–181.

Kleeman, M. J., and G. R. Cass, 2001: A 3D Eulerian source-oriented model for an externally mixed aerosol. *Environ. Sci. Technol.,* **35,** 4834–4848.

Kuwagata, T., and F. Kimura, 1997: Daytime boundary layer evolution in a deep valley. Part II: Numerical simulation of the cross-valley circulation. *J. Appl. Meteor.,* **36,** 883–895.

Leung, L. R., and S. Ghan, 1999: Pacific Northwest climate sensitivity simulated by a regional climate model driven by a GCM. Part II: 2 $\times$ CO_2 simulations. *J. Climate,* **12,** 2031–2053.

——, and W. I. Gustafson Jr., 2005: Potential regional climate change and implications to U.S. air quality. *Geophys. Res. Lett.,* **32,** L16711, doi:10.1029/2005GL022911.

Mahmud, A., M. Tyree, D. Cayan, N. Motallebi, and M. J. Kleeman, 2008: Statistical downscaling of climate change impacts on ozone concentrations in California. *J. Geophys. Res.,* **113,** D21103, doi:10.1029/2007JD009534.

——, M. Hixson, J.-L. Hu, Z. Zhao, S.-H. Chen, and M. J. Kleeman, 2010: Climate impact on airborne particulate matter concentrations in California using seven year analysis periods. *Atmos. Chem. Phys.,* **10,** 11 097–11 114.

Mellor, G. L., and T. Yamada, 1982: Development of a turbulence closure model for geophysical fluid problems. *Rev. Geophys.,* **20,** 851–875.

Michalakes, J., S.-H. Chen, J. Dudhia, L. Hart, J. Klemp, J. Middlecoff, and W. Skamarock, 2001: Development of a next generation regional weather research and forecast model. *Developments in Teracomputing: Proceedings of the Ninth ECMWF Workshop on the Use of High Performance Computing in Meteorology,* W. Zwieflhofer and N. Kreitz, Eds., World Science, 269–276.

Mlawer, E. J., S. J. Taubman, P. D. Brown, M. J. Iacono, and S. A. Clough, 1997: Radiative transfer for inhomogeneous atmosphere: RRTM, a validated correlated-*k* model for the longwave. *J. Geophys. Res.,* **102,** 16 663–16 682.

Mölders, N., and G. Kramm, 2009: A case study on wintertime inversions in Interior Alaska with WRF. *Atmos. Res.,* **95,** 314–332.

Pierce, D. W., T. P. Barnett, R. Tokmakian, A. Semtner, M. Maltrud, J. Lysne, and A. Craig, 2004: The ACPI Project, element 1: Initializing a coupled climate model from observed conditions. *Climatic Change,* **62,** 13–28.

Saha, S., and Coauthors, 2006: The NCEP Climate Forecast System. *J. Climate,* **19,** 3483–3517.

Singal, S. P., S. K. Aggarwal, and D. R. Pahwa, 1986: Studies of the marine boundary layer at Tarapur. *Bound.-Layer Meteor.,* **37,** 371–384.

Skamarock, W. C., J. B. Klemp, J. Dudhia, D. O. Gill, D. M. Barker, W. Wang, and J. G. Powers, 2007: A description of the advanced research WRF version 2. NCAR Tech. Note NCAR/TN-468+STR, 88 pp.

Snyder, M. A., J. L. Bell, L. C. Sloan, P. B. Duffy, and B. Govindasamy, 2002: Climate responses to a doubling of atmospheric carbon dioxide for a climatically vulnerable region. *Geophys. Res. Lett.,* **29,** 1514, doi:10.1029/2001GL014431.

Tagaris, E., K. Manomaiphiboon, K.-J. Liao, L. R. Leung, J.-H. Woo, S. He, P. Amar, and A. G. Russell, 2007: Impacts of global climate change and emissions on regional ozone and fine particulate matter concentrations over the United States. *J. Geophys. Res.,* **112,** D14312, doi:10.1029/2006JD008262.

Thompson, G., R. M. Rasmussen, and K. Manning, 2004: Explicit forecasts of winter precipitation using an improved bulk microphysics scheme. Part I: Description and sensitivity analysis. *Mon. Wea. Rev.,* **132,** 519–542.

Washington, W. M., and Coauthors, 2000: Parallel climate model (PCM) control and transient simulations. *Climate Dyn.*, **16,** 755–774.

Whiteman, C. D., 1982: Breakup of temperature inversions in deep mountain valleys: Part I. Observations. *J. Appl. Meteor.,* **21,** 270–289.

Wilby, R. L., T. M. L. Wigley, D. Conway, P. D. Jones, B. C. Hewitson, J. Main, and D. S. Wilks, 1998: Statistical downscaling of general circulation model output: A comparison of methods. *Water Resour. Res.,* **34,** 2995–3008.

Zhang, Y., M. K. Dubey, and S. C. Olsen, 2009: Comparisons of WRF/Chem simulations in Mexico City with ground-based RAMA measurements during the MILAGRO-2006 period. *Atmos. Chem. Phys. Discuss.,* **9,** 1329–1376.

Zhao, Z., S.-H. Chen, M. J. Kleeman, and A. Mahmud, 2011: The impact of climate change on air quality–related meteorological conditions in California. Part II: Present versus future time simulation analysis. *J. Climate,* in press.

Zorita, E., and H. von Storch, 1999: The analog method as a simple statistical downscaling technique: Comparison with more complicated methods. *J. Climate,* **12,** 2472–2487.